**Structural Engineering and Mechanics**, *Vol. 47, No. 6 (2013) 741-756*
DOI: http://dx.doi.org/10.12989/sem.2013.47.6.741


# Experimental and analytical investigation on RC columns with distributed-steel bar

Mao Ye*, Yinpei Pi[a] and Min Ren[b]

*Guangzhou University – Tamkang University Joint Research Center for Engineering Structure Disaster Prevention and Control, Guangzhou University, 230 Wai Huan Xi Road, GuangZhou Higher education Mega Center, GuangZhou, Guangdong Province, PR China*

*(Received April 29, 2012, Revised April 16, 2013, Accepted August 30, 2013)*

**Abstract.** Distributed-Steel Bar Reinforced Concrete (DSBRC) columns, a new and innovative construction technique for composite steel and concrete material which can alleviate the difficulty in the arrangement of the stirrup in the column, were studied experimentally and analytically in this paper. In addition, an ordinary steel Reinforced Concrete (SRC) column was also tested for comparison purpose. The specimens were subjected to quasi-static load reversals to model the earthquake effect. The experimental results including the hysteresis curve, resistance recession, skeleton curves and ductility ratio of columns were obtained, which showed well resistant-seismic behavior for DSBRC column. Meanwhile a numerical three-dimensional nonlinear finite-element (FE) analysis on its mechanical behavior was also carried out. The numerically analyzed results were then compared to the experimental results for validation. The parametric studies and investigation about the effects of several critical factors on the seismic behavior of the DSBRC column were also conducted, which include axial compression ratios, steel ratio, concrete strength and yield strength of steel bar.

**Keywords:** reinforced concrete columns; distributed–steel Bar; finite element method; axial loads; seismic effects

## 1. Introduction

Steel Reinforced Concrete (SRC) columns are composite columns with both steel and concrete materials resisting compressive force and bending moment simultaneously. Compared with pure steel and reinforced concrete, SRC offers several advantages in its structural behavior (Ehab and Ben 2006, Uy 2001). The stiffness of SRC column is greatly enhanced by the reinforced steel within its section. Also the lateral confinement provided by the steel reinforcement improves the strength, ductility and deformability of the concrete. Reinforcement detail together with the concrete in the cross-section can optimize the strength and stiffness of the section.

In recent years, SRC columns have been increasingly used in the structures due to their beneficial properties (Ehab and Ben 2006, Uy 2001). Also, a large number of studies were carried

∗Corresponding author, Ph.D., E-mail: yemao@gzhu.edu.cn
[a]M.E. Student, E-mail: 382491697@qq.com
[b]Professor, E-mail: rm_58@163.com


http://www.techno-press.org/?journal=sem&subpage=8 ISSN: 1225-4568 (Print), 1598-6217 (Online)

out on SRC columns, especially for tubed steel columns (Shanmugam and Lakshmi 2001, Zeghiche 1998, Shakir and Mouli 1990) and reinforced-concrete filled-steel tubular columns (Zhao *et al*. 2005, Wang *et al*. 2004). Chang *et al.* (2012) presented a new form of composite column: Reinforced-Concrete Filled-Steel Tubular column (RCFST), and Qi *et al*. (2011) carried out experiments to investigate the failure mode and axial loaded behavior of some circular and square tubed SRC stub columns. Their results indicated that tubed SRC stub columns obtain higher axial load capacity than common SRC columns. Yu *et al*. (2008) conducted the tests on 28 thin-walled hollow structural steel columns filled with ultra-high strength self-consolidating concrete. Their test results indicated that the existing codes, such as ANSI/AISC (2005) and Eurocode 4 (1994), are acceptable for predicting the member capacities of high strength SCC filled HSS columns. Tokgoz *et al*. (2010) have conducted an experimental study about steel tubular columns in-filled with plain and steel fiber reinforced concrete; their results indicated that the additional steel fibers in core concrete have considerable effect on the behavior of concrete-filled steel tube columns. In addition to experimental tests, numerical analysis is an important tool to elucidate further information about the behavior of SRC columns under limited budgets. Tao *et al*. (2011), Han *et al*. (2008) and Hu *et al*. (2005) have developed models of Concrete-Filled Steel Tubes (CFSST) by ABAQUS. The strengthening effect of reinforced concrete (RC) columns with Fiber-Reinforced Polymer (FRP) composites has also been numerically modeled by three-dimensional nonlinear finite element (FE) method (Doran *et al*. 2009, Rougiera and Luccionia 2007).

In the last few years, there are a wide variety of SRC columns with varying cross-section, such as encased I-section, rectangle, bi-channel, four-angle, steel tubes etc. However, some complaints also have been reported that the difficulty exist in the arrangement of stirrup in the column and longitudinal reinforcement in the beam, which leads to difficult construction and high cost (Bu 2010). Based on the principle with the equal ratio in reinforced steel, a new and innovative construction technique, which called as Distributed Steel Bar Reinforced Concrete (DSBRC) column, emerged as one of the effective choices. There are many practical applications of DSBRC columns adopted in self-bearing members in civil engineering, and their effects are obvious. As the lack of proper seismic provisions in their design, a comprehensive evaluation on these columns is necessary to understand the behavior of DSBRC columns subjected to seismic effects.

The present study tried to conduct experimental and finite-element (FE) analysis to improve the information about the seismic behavior of DSBRC columns. The first part contains the test results of two specimens, a DSBRC column and a SRC column with same square cross-section. The test was conducted under quasi-static cyclic load reversals to simulate seismic effect. The comparison in the behavior of energy dissipation, skeleton curves, strength, stiffness degradation and ductility between DSBRC and SRC are conducted in this paper. The second part of the study includes the comparison of the experimental results with numerical FE analysis, and a critical parametric study was performed to elucidate further information, such as the effect of axial compression ratios, steel ratio, the strength of concrete and the yield strength of steel bar on the seismic behavior of the DSBRC column.

## 2. Test program

### *2.1 Specimen Details*

Figs. 1-2 show the details of the two test specimens with a rectangular cross section of 300×300

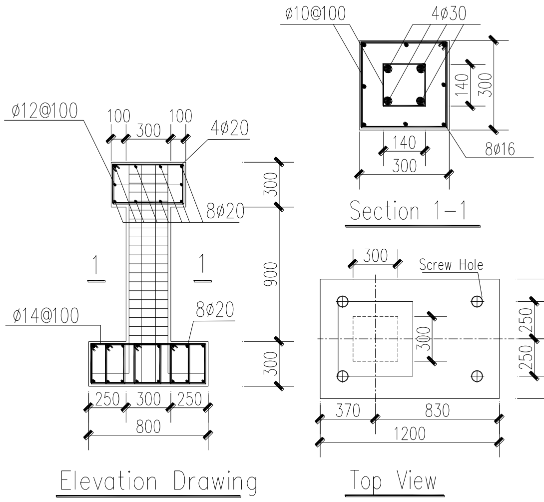


Fig. 1 DSBRC column, SRC-1

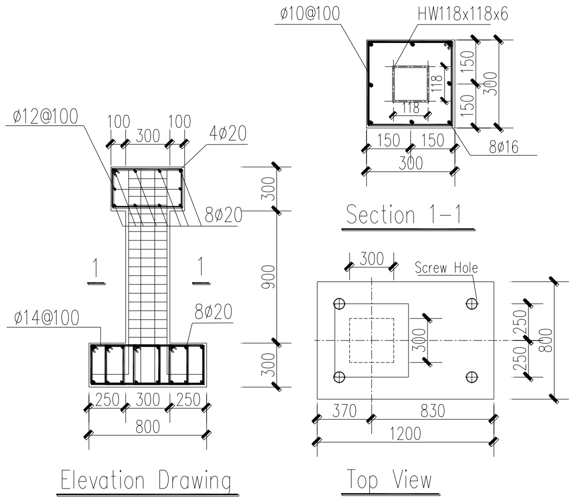


Fig. 2 Ordinary SRC column, SRC-2

Table 1 Test matrix

| Specimen ID | Shear span ratio | Designed axial compression ratio | Steel ratio | Longitudinal reinforcement ratio | Volume ratio of reinforcement |
|---|---|---|---|---|---|
| SRC-1 | 2.5 | 0.7 | 3.14% | 1.79% | 0.93% |
| SRC-2 | 2.5 | 0.7 | 3.20% | 1.79% | 0.93% |

* SRC-1: DSBRC column; SRC-2: Ordinary SRC column

mm and height in 900 mm. They are labeled as SRC-1 and SRC-2 for DSBRC column, ordinary SRC column respectively. The shear span ratio, designed axial compression ratio, longitudinal reinforcement ratio and volume ratio of reinforcement used in specimens are summarized in Table 1. On the making process for the two test specimens, the right position of the steel bars, shaped-steels, reinforcements and the interval between the successive pouring should be carefully controlled.

### *2.2 Material properties*

Ready-mix concrete with a nominal 80 MPa compressive strength was used to cast the column specimens. Three standard test specimens (150×150×150 mm) were also cast which were tested under compression after 28 days' curing according to the Standard Methods for Testing of Concrete Structures (GB50152-92). The average compressive strength of concrete, $f_{ck}$, was found to be 81.1 MPa for tested specimens. The elastic modulus $E_C$ is 38.2GPa and the density is 2425 kg/m$^3$. Columns were reinforced by 4 A45 (30-mm in diameter) steel bars for DSBRC column and Q235 steel hellow tubular (square cross section of 118×118 mm and a thickness of 6 mm) for ordinary SRC column. The materials of stirrups and longitudinal reinforcements for two test specimens are HRB335 (10mm diameter), HRB400II (16mm diameter) respectively. The nominal yield and ultimate strengths of the steel bars, steel tubular, longitudinal reinforcements and stirrups are listed in Table 2.

Table 2 Properties of A45steel bar, Q235steel tubular, HRB400II and HRB335

| A45 Steel Bar | | Q235 Steel Tubular | | HRB400II | | HRB335 | |
|---|---|---|---|---|---|---|---|
| Yield strength | Ultimate strength | Yield strength | Ultimate strength | Yield strength | Ultimate strength | Yield strength | Ultimate strength |
| 355MPa | 600MPa | 235MPa | 375MPa | 400MPa | 540MPa | 335MPa | 455MPa |

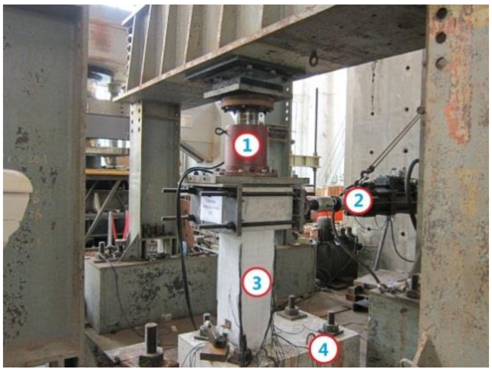


Fig. 3 Test setup

### *2.3 Test setup*

Fig. 3 shows the conducted test in the Earthquake Engineering Research & Test Center of Guangzhou University, Guangzhou. The test specimens were subjected to quasi-static load reversals for modeling the earthquake effect. A hydraulic jack with 320 ton capacity was utilized to apply vertical axial compressive force to the column specimens and a hydraulic jack with 50 ton capacity to apply lateral force. A displacement transducer was installed at top of the column specimens to measure the lateral displacement, and two tilters were installed at the bottom of the column specimens to measure the rotation. In addition, strain gauges were used to record the strains level of steel reinforcement during the experiment. The load cell and the transducers were calibrated before they were used in the tests. A data acquisition system was arranged to collect the applied load, the lateral deflections, and the strain measurements.

Test specimens were tested under Specification of Testing Methods for Earthquake resistant building (JGJ 101-96). Prior to testing, the top level of the columns was axially loaded initially to eliminate the uneven distribution of specimens. The axial load was then applied to the column specimens until the designed axial compression ratio was met. Secondly, Lateral loads by increment of 50kN in 3 recycles were applied before the column yielded. Then specimens were loaded under displacement control at the top of column until failure.

### *2.4 Test results and analysis*

#### *2.4.1 Failure modes*

Typical failure state with ductile compression-bending failure mode was shown in the test specimens in Fig. 4. The maximum bearing capacity was approximately 242.7 kN for DSBRC column and 272.4 kN for square cross-section SRC column. Until the specimen was loaded at 67% or 61.8% of their maximum capacities, columns SCR-1, SCR-2 experienced the initial flexural and

(a) SRC-1

(b) SRC-2

Fig. 4 Failure modes

shear cracks simultaneously. In the successive loading levels, some vertical compression cracks were developed at the bottom of the columns, and the steel bars carried more shear force in test specimen. With the increased loading, the plastic hinge appeared and reinforcement and steel began to yield. The lateral load decreased gradually after its peak values reached. When the specimen experienced a more than 20% loss in its load-bearing capacity, the test stopped. At this stage, spalling of concrete at the column compression zone was observed in Fig. 4 due to crushing effect.

### *2.4.2 Hysteretic curves of load-displacement*

Fig. 5 shows the hysteresis curves of SRC-1 and SRC-2 under lateral loads versus the lateral displacement. $P_o$, $P_y$, $P_u$, $P_m$ are the crack load, yield load, peak load and 85% of the peak load. In the successive loading cycles, SRC-1 reached its maximum capacities with approximately 242.3 kN in the initial loading direction and 308.7kN in the reverse-loading direction, with corresponding Lateral displacements in 17mm and 19mm, respectively. The corresponding maximum capacities for SCR-2 are approximately 278.6kN and 275.9kN respectively, along with Lateral displacement in 21.6mm and 16.9mm, respectively. The bearing capacity of SRC-2 was 13.8% and 10% higher than those values for Specimen SCR-1 in two directions. The specimen showed a significant pinching behavior throughout the test.

With the areas covered by the load-displacement curves in Fig. 6, the specimens' capacity for energy dissipation was expressed in terms of the energy dissipation coefficient E in the following

$$E = S_{(ABC+CDA)} / S_{(\Delta OBE+\Delta ODF)} \tag{1}$$

The relationship between $E$ and the displacement at the last controlled displacement was shown in Fig. 7 for all specimens. Energy dissipation coefficient $E$ increases as the displacement increases for all specimens. The energy dissipation capacity for the DSBRC column seems to performance as excellent as that of squared cross-section SRC column.

In general, the hysteretic curves are plump. Energy dissipation capacity for these columns was equally excellent.

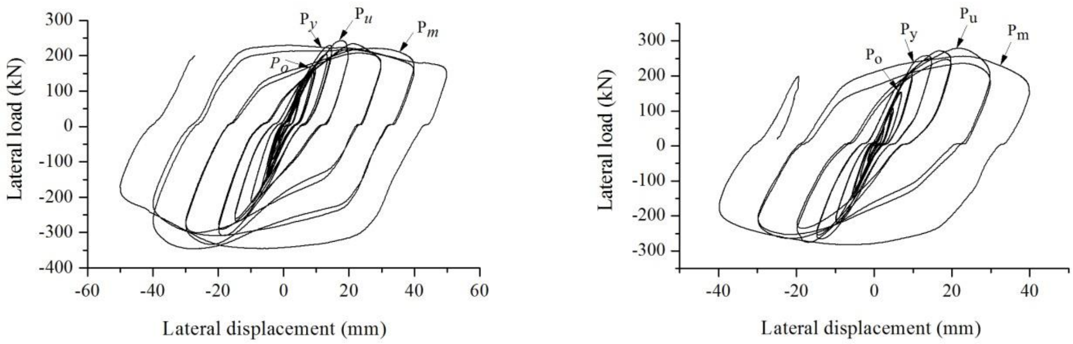


(a) SCR-1 (b) SCR-2

Fig. 5 Hysteretic behavior

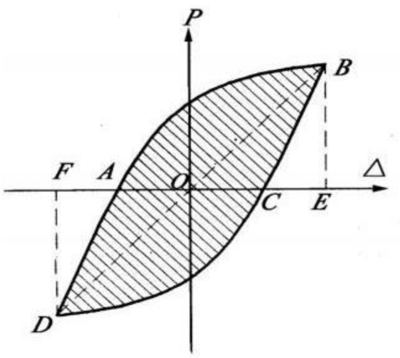


Fig. 6 Load-displacement curve

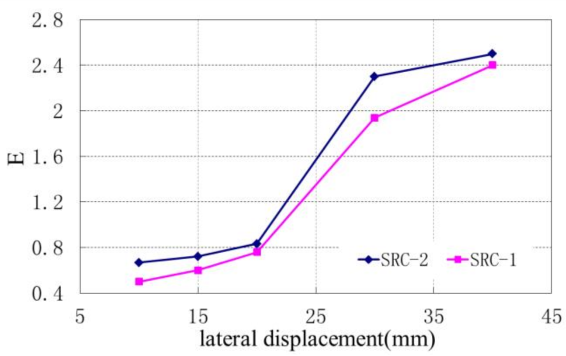


Fig. 7 The energy dissipation coefficient- displacement curve

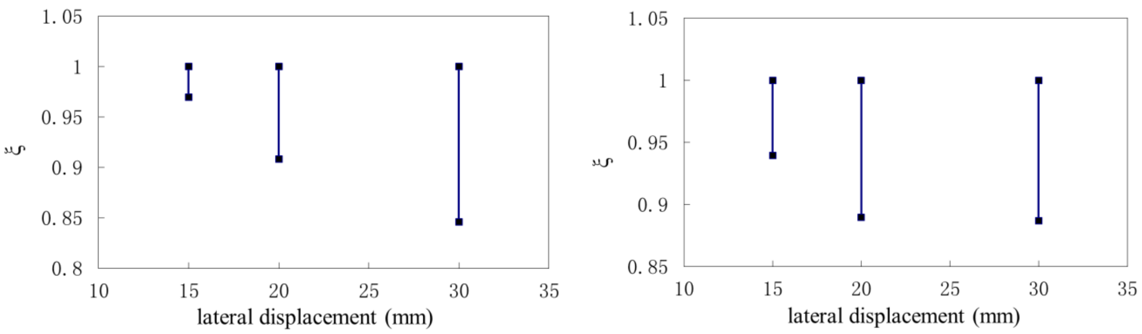


(a) SRC-1 (b) SRC-2

Fig. 8 $\zeta_i$ - displacement curves

*2.4.3 Strength degradation*

The strength degradation coefficient $\zeta_i$ (Zheng and Ji 2008), defined as the ratio of the peak load at the *i*th cycle to the first cycle under the same controlled displacements. The relationship between $\zeta_i$ and controlled displacements for SRC-1 and SRC-2 was shown in Fig. 8. It was shown

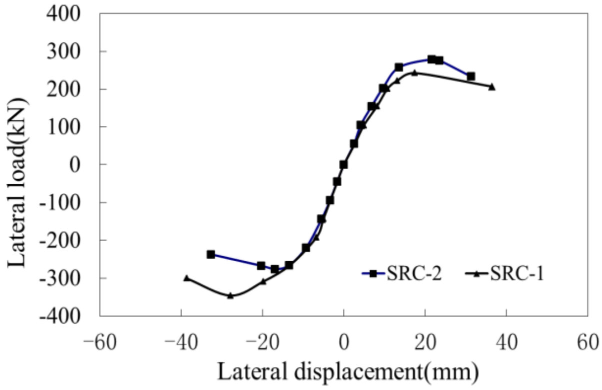


Fig. 9 Skeleton curves

Table 3 The displacement ductility coefficient

| Specimen ID | Axial compressive ratio | Steel ratio | $\Delta_u$(mm) | $\Delta_y$(mm) | Displacement ductility coefficient $\mu$ |
|---|---|---|---|---|---|
| SRC-1 | 0.30 | 3.14% | 12.1 | 38.9 | 4.20 |
| SRC-2 | 0.32 | 3.20% | 10.5 | 31.8 | 3.25 |

that the strength degradation increased with the increasing displacement. The strength degradation coefficient for DSBRC column decreased more rapidly than square cross-section SRC column.

### *2.4.4 Skeleton curve*

The skeleton curve is a type of curve defined as the variation of the maximum load with the controlled displacement, which were selected from the peak values in the first cycle under the cyclic loading experiment. The skeleton curves for SRC-1 and SRC-2 (shown in Fig. 9) demonstrated that the bearing capacity of SRC-1 declines more slowly after the ultimate load reached. However, ultimate bearing capacity of SRC-2 is relatively larger.

### *2.4.5 Ductility*

The displacement ductility coefficent is defined as the ratio of the ultimate displacement $\Delta_u$ to the yielding displacement $\Delta_y$. The yielding displacement $\Delta_y$ can be obtained from the energy method, and the ultimate displacement is generally assumed to be the displacement at the descending segment curve when 85% of the peak load reached (Zheng and Ji 2008). The estimated displacement ductility coefficients for all specimens are listed in Table 3, which showed that the ductility performance of SRC-1 is better than SRC-2.

From the failure mode, hysteretic curves, strength degradation ($\zeta$) and ductility ($\mu$) observed in the tests, it was demonstrated that DSBRC column showed as good seismic behavior as the square cross-section SRC column under cyclic loading, but, it can alleviate the difficulty for the arrangement of stirrup in the column and the longitudinal reinforcement in the beam. Therefore it would be suitable substitute of SRC column in civil engineering.

## 3. Nonlinear finite-element analysis

### 3.1 Finite element modeling

#### 3.1.1 General

The following sections presented the numerical 3D nonlinear FE simulation on the seismic behavior of DSBRC column in order to enhance the understanding about its complex behavior. In this study, ABAQUS, a general-purpose FE program, was employed for the numerical simulation. In the FE model, the cross-section dimensions and material properties from the tests were modeled. The constitutive model for the concrete and steel material inherent in this software package was adopted in our analysis. They are described in ABAQUS theory and modeling guide, and briefly summarized in the following section.

#### 3.1.2 Element type and mesh

To simulate the real behavior of tested DSBRC column, it is imperative that the concrete column be modeled by solid elements-C3D8R in ABAQUS, which is 8-node brick, first-order and reduced-integration element with hourglass control in three dimensions. The reason for this selection is that brick elements can produces the best results with the minimum costs in three-dimensional analyses. To model the behavior of steel reinforcement, T3D2 (a 2-node straight truss element) is adopted with linear interpolation in coordinate and displacement to obtain a constant stress state. The finite element mesh used in the model was investigated by varying the size of the elements in the cross-section. It was found that good simulation results could be obtained by using the element size of approximately 30mm×30mm (length by width) and 30 mm for C3D8R and T3D2, respectively. Bond-slip behavior for DSBRC column did not be considered in the FE model. Typical meshes of specimens are shown in Fig. 10.

#### 3.1.3 Boundary condition, method of loading

The fixed-ended boundary condition was modeled by restraining all the degrees of freedom of the nodes at the bottom surface of DSBRC columns. The free boundary condition was modeled at the top surface of DSBRC columns. The loading method used in the FE analysis was identical to that used in the experiments. The top of DSBRC column was axially loaded at a constant when the experimental axial compression ratio was met. The displacement control method was used for lateral loading. The FE models were subjected to a cyclically increasing lateral load.

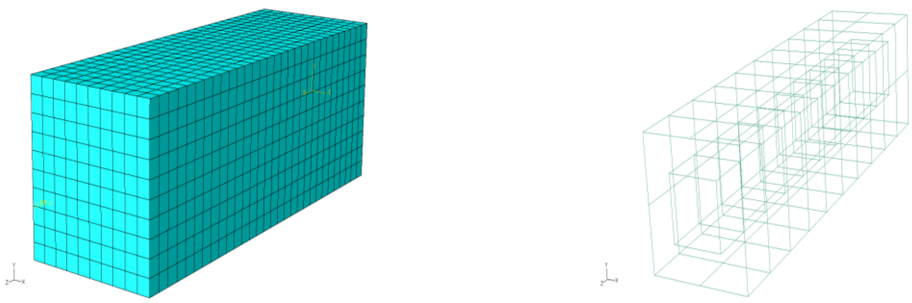

(a) C3D8R for concrete (b) T3D2 for steel reinforcement (layout in column)

Fig. 10 Finite element meshes in the three-dimensional finite-element model

Table 4 Parameters about the plasticity damaged model (in ABAQUS)

| Dilation angle | Eccentricity | The ratio of initial equibiaxial compressive yield stress to initial uniaxial compressive yield stress | The ratio of the second stress invariant on the tensile meridian to that on the compressive meridian | Viscosity Parameter |
|---|---|---|---|---|
| 30 | 0.1 | 1.16 | 0.667 | 0.001 |

### *3.1.4 Material constitutive models for concrete and reinforcing steel*

The plasticity damaged model (ABAQUS 2004) for concrete was adopted in this paper, which is also suitable for the analysis for quasi-brittle materials, such as rock, mortar and ceramics. This constitutive model can simulate the effects of irreversible damage which is related with the failure mechanisms occurred in concrete under fairly low confining pressures. Moreover, the non-associative plasticity flow rule and the Drucker–Prager yield criteria are assumed in this model. It also adopts a yield criteria proposed by Lubliner *et al*. (1989) and incorporates its modifications proposed by Lee and Fenves (1998) to account for different evolution of strength in tension and compression state. The compressive stress–strain relationship for confined concrete is selected from Mander *et al*. (1988), which is widely accepted and expressed in terms of a single curve shown in Fig. 11. The main equations are given below

$$\sigma_c = \frac{\sigma_{cc} x r}{r - 1 + x^r} \tag{2}$$

where $x = \varepsilon_c / \varepsilon_{cc}$ , $r = E_c / (E_c - E_{\text{sec}})$ , $E_{\text{sec}} = f_{cc} / \varepsilon_{cc}$ , $E_c = 5000\sqrt{\sigma_{c0}}$ is the tangent elasticity modulus of the concrete where $E_c$ and $\sigma_{c0}$ in MPa unit. $\sigma_{cc}$ is the compressive strength of confined concrete and $\varepsilon_{cc}$ is the corresponding strain , defined as

$$\sigma_{cc} = \sigma_{co}\left(2.254\sqrt{1 + \frac{7.94\sigma_l}{\sigma_{co}}} - 2\frac{\sigma_l}{\sigma_{co}} - 1.245\right) \tag{3}$$

$$\varepsilon_{cc} = \varepsilon_{co}\left[1 + 5\left(\sigma_{cc} / \sigma_{co} - 1\right)\right] \tag{4}$$

where $\sigma_{co}$ is the unconfined concrete compressive strength and $\varepsilon_{co}$ is the corresponding strain. $\sigma_l$ is the effective lateral confining stress on the concrete.

In Fig. 11, ultimate compressive strain for concrete $\sigma_{cu}$ is defined by Code for China Design of Concrete Structures (GB 50010 - 2010). Concrete in tension is neglected after its cracking. Some parameters about the plasticity damaged model (in ABAQUS) are displayed in Table 4.

For reinforcing steel, the von Mises yield criterion with isotropic strain hardening and an associated flow rule were adopted to describe its constitutive behavior. Fig. 12 showed the stress-strain relationship for the reinforcing steel (Lu *et al*. 2007). $f_p$ , $f_y$ , $f_u$ are proportion limit, yield strength, tensile strength respectively. There is perfect bond between the longitudinal reinforcing steel bars and the concrete.

### *3.2 Verification of finite-element model*

The load–displacement curves of DSBRC column obtained from the test and finite element analysis by ABAQUS as well as the ultimate lateral loads have been investigated. The curves for lateral load ($F$) versus lateral displacement ($\Delta$) of the tested DSBRC column from FE analysis are plotted in Fig. 13 together with its experimental envelop curves. Hysteretic curves are presented in Fig. 14. It can be shown that good agreement has been generally achieved between the analytical and the experimental results.

As shown from Fig. 13, the load-bearing capacities of the tested specimens were slightly higher at early stages. At a displacement of 3.2mm, the FE analysis result exceeded the tested results and reached its ultimate capacity at the displacement of approximately 6.9mm, which was about 2.8% higher than the measured value. Thereafter, moderate strength and stiffness degradations were founded. From the previous discussions, the FE model is obviously acceptable despite some minor differences; therefore the numerical analysis results can be adopted to predict the seismic behavior of DSBRC column.

### *3.3 Parametric studies*

This section showed a parametric study to elucidate more information about the complex behavior of the DSBRC columns. The structural response of the columns was studied by varying

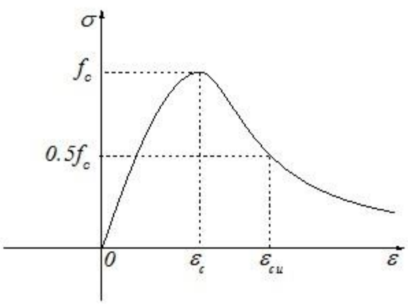


Fig. 11 Compressive stress-strain relationship for concrete

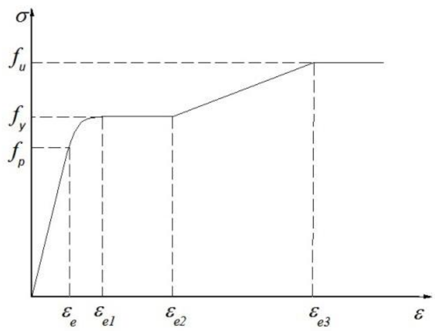


Fig. 12 Stress-strain curves for steel

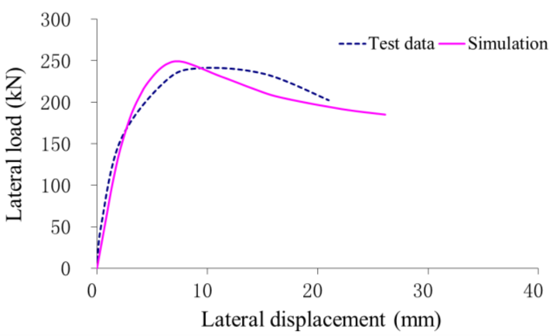


Fig. 13 Comparisons of lateral load versus displacement curves for SRC-1

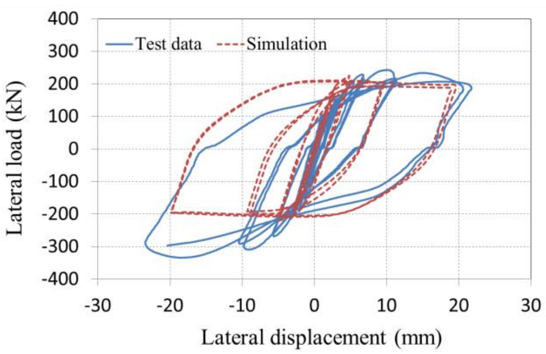


Fig. 14 Lateral force-displacement hysteretic curve

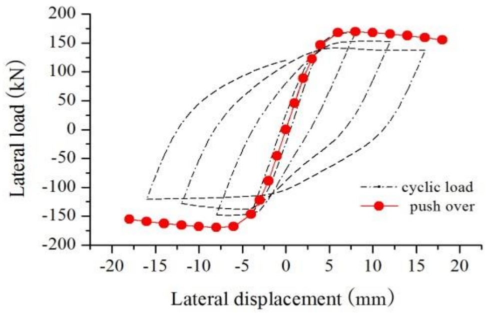


Fig. 15 Comparisons between hysteretic curves and monotonically load-displacement curve

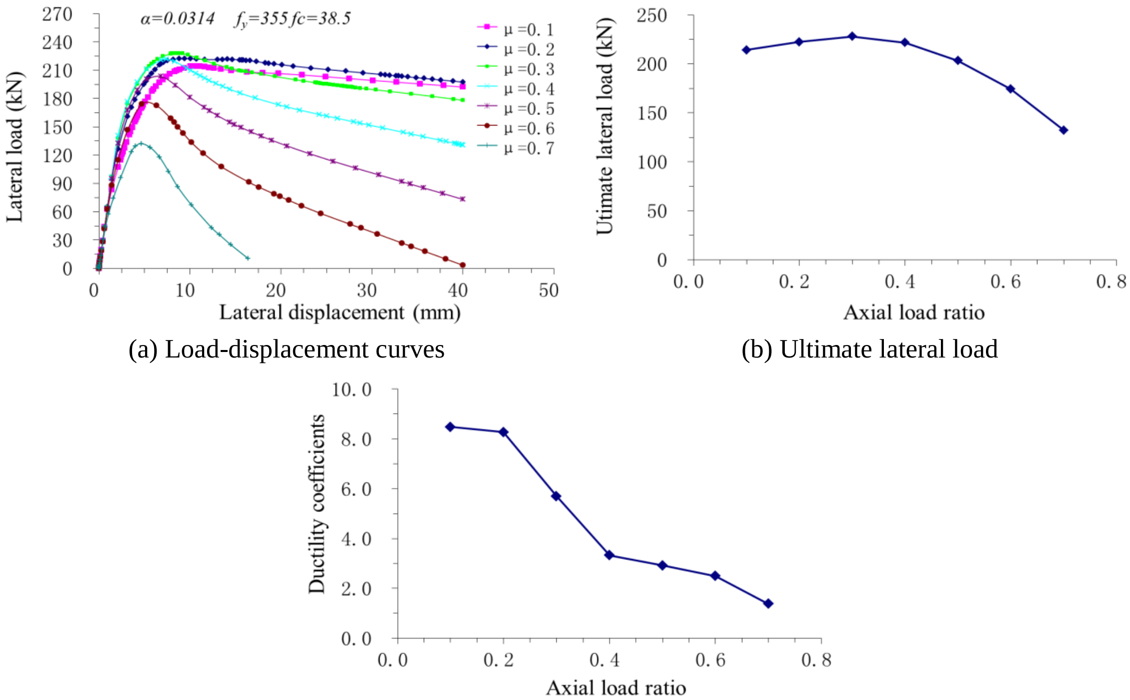


(a) Load-displacement curves (b) Ultimate lateral load

(c) Ductility coefficient

Fig. 16 The effect of axial load ratios

some key parameters such as axial load ratio, steel ratio, concrete compressive strength and steel yield strength.

The seismic behavior of column was shown primarily from the skeleton curve under cyclic loading. Existed research results have shown that the skeleton curve was almost coincided with load-displacement curve under monotonic loading (Zhang 2001). Another verifiable model (not SRC-1 or SRC-2) is built by the author; Fig. 15 showed the corresponding results which are consistent with the existing research studies. Therefore, the monotonic loading was adopted to study the seismic behavior of DSBRC columns instead of cyclic loadings.

### *3.3.1 Effect of axial load ratio*

The load-displacement curve, ultimate Lateral load and ductility coefficient under different axial load ratios were plotted in Fig. 16. The column carried the axial load from 0.1 to 0.7$f_c$ $A_g$ levels ($A_g$: the area of the cross section of column). As observed from Fig. 16(b), the ultimate lateral load of DSBRC column increased by about 6.5% with axial load ratio increased from 0.1 to 0.3. However, the ultimate lateral loads of DSBRC column decreased by about 42.1% when axial load ratios increased from 0.3 to 0.7. Any increase in the axial load ratio results in the stiffness degradation and further reduction in the ultimate lateral load as shown in Fig. 16(a)-(b) respectively. The ductility for DSBRC columns degraded monotonously as the axial load ratio increased. Ductility coefficients reduced from 5.52 to 1.42 with the increasing axial load ratios.

### *3.3.2 Effect of steel ratio*

The effect of steel ratio on load-displacement curve, ultimate lateral load and ductility coefficient were presented in Fig. 17 with the steel ratio varying from 0.02 to 0.08. As steel ratio increased, the load-displacement behavior of the DSBRC columns is similar to the bilinear elastic-plastic material shown in Fig. 17(a). At the steel ratio of 0.08, the deformation hardening stage occurred obviously, which reflects the mechanical behavior of steel. No significant effects of the steel ratio on the ultimate lateral load of DSBRC column was found in Fig. 17(b). Ultimate lateral load increased around 21% with the increasing steel ratio from 0.02 to 0.08. Meanwhile ductility coefficient increased by around 301.2% as shown in Fig. 17(c), which indicated that the effect of steel ratio on the ductility coefficient of DSBRC columns is very significant.

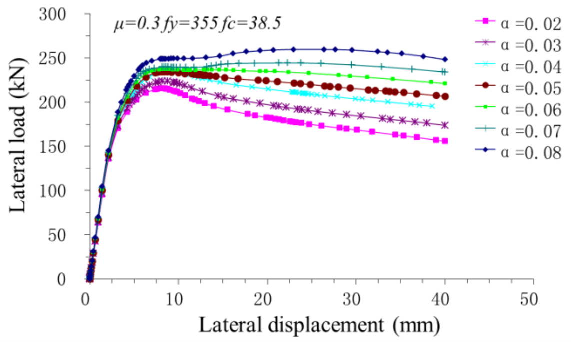


(a) Load-displacement curves

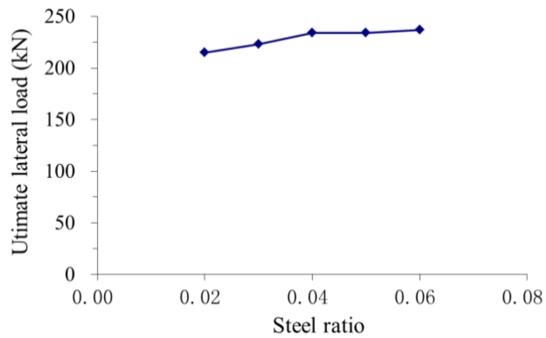


(b) Ultimate lateral load

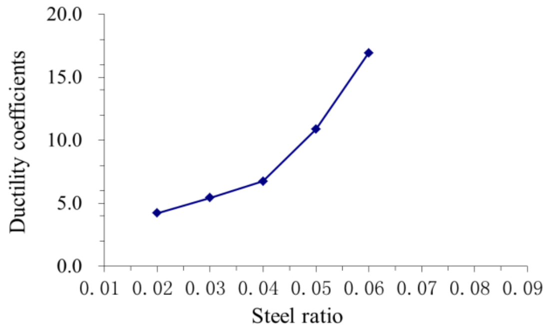


(c) Ductility coefficient

Fig. 17 The effect of steel ratios

1: Vertical hydraulic jack

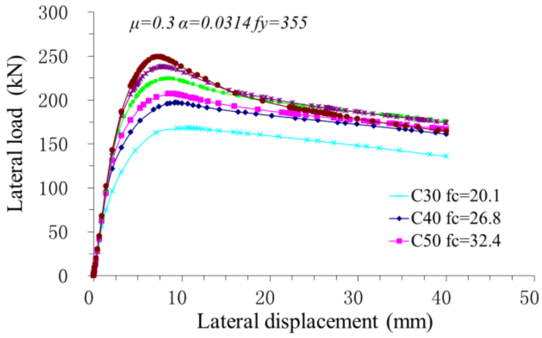


(a) Load-displacement curves

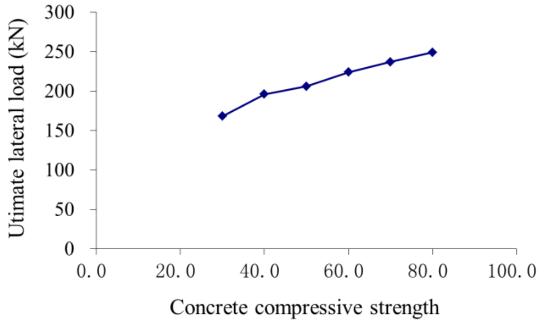


(b) Ultimate lateral load

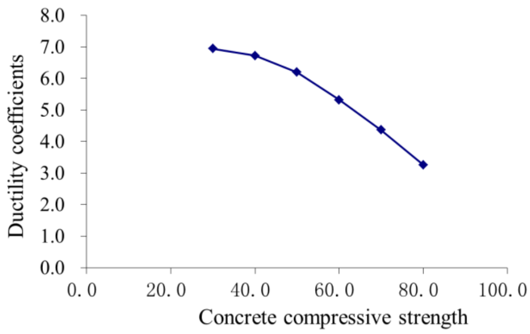


(c) Ductility coefficient

Fig. 18 Effect of concrete nominal strength

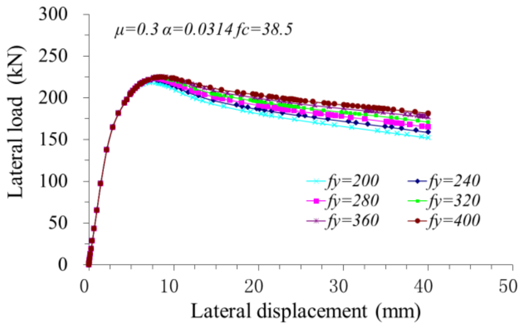


(a) Load-displacement curves

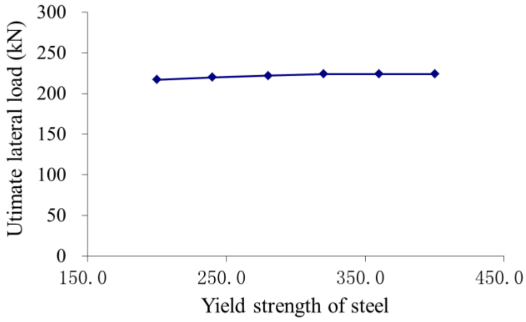


(b) Ultimate lateral load

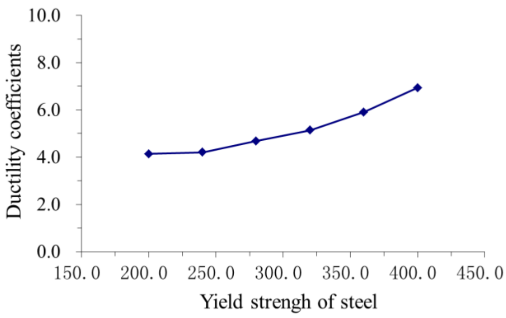


(c) Ductility coefficient

Fig. 19 Effect of yield strength

1: Vertical hydraulic jack

### *3.3.3 Effect of concrete compressive strength*

Figs. 18 present the effect of concrete compressive strength on load-displacement curve, ultimate lateral load and ductility coefficient. As shown in Figs. 18(b)-(c), the concrete compressive strength has an obvious effect on the ultimate Lateral load and the ductility coefficient of DSBRC columns. As concrete nominal strengths increased from C30 to C80, ultimate lateral loads was increased by around 48.5%. But ductility coefficient decreased by around 52.5% correspondingly.

### *3.3.4 Effect of yield strength of steel*

The load-displacement curve, ultimate lateral load and ductility coefficient were shown in Fig. 19 under various yield strengths of distributed-steel bar. The effect of steel yield strength on the ultimate lateral load is not obvious. The ultimate lateral load increased only 3.2% as the nominal steel yield strength varied from 200 MPa to 400 MPa. However, the effect of steel yield strength on ductility coefficient is much larger.

## 4. Conclusions

The behavior of reinforced concrete column with the distributed-steel bar under vertical and incremental lateral loadings was analyzed in this paper. Through experimental test and numerical FE analysis, the conclusions can be summarized as the following:

• Both energy dissipation capacity of DSBRC column and ordinary SRC column are excellent. The ultimate bearing capacity of DSBRC column is slightly less and its strength degradation coefficient decreases more sharply. However, its ductility performance is superior to that of the squared cross-section SRC column.

• The effect of axial load ratio on the ultimate lateral load, the stiffness degradation and the ductility performance of DSBRC column were studied comprehensively in this paper.

• Meanwhile the effect of steel ratios on the load-displacement behavior, the ultimate Lateral load and ductility coefficient of the DSBRC column were studied in this paper. Some valuable conclusions were also found.

• The effect of the nominal concrete compressive strength on the ultimate Lateral load and its ductility coefficient of DSBRC columns are obvious. The effect of yield strength on the ultimate Lateral load is not obvious, but its effect on ductility coefficient is much larger.

• Comparison between the numerical FE analysis results with the experimental test verified that the proposed numerical approach is appropriate for estimating the seismic behavior of DSBRC columns.

• Experimental test results showed that DSBRC column presented good seismic behavior under cyclic loading as the ordinary SRC column, but it can alleviate the difficulty in construction of reinforcement in DSBRC column. Therefore it would be a good substitute of SRC column in civil engineering construction.

## Acknowledgments

The experimental test was carried out at the Earthquake Engineering Research & Test Center of Guangzhou University, Guangzhou University, Guangzhou. The conducted research work in this paper was funded by China National Natural Fund (Project No. 51178126, 51208125), Science and Technology Program of Guangzhou, China (Project No. 2013J2200074) and Guangdong science and technology plan (Project No. 2009B050200015), and the financial supports were gratefully acknowledged.

## References

ABAQUS Inc (2004), *ABAQUS Theory Manual And User Manuals, Version 6.5*, R.I. ABAQUS Inc., Providence, USA

ANSI/AISC 360-05 (2005), *Specification for structural steel buildings,* American Institute of Steel Construction, Chicago, USA.

Bu, N. (2010), "Construction technology of steel-concrete composite structure in China World Trade Center Tower Ⅲ project", *Construction Technology*, **39**(10), 89-92. (in Chines)

Chang, X., Wei, Y.Y. and Yun, Y.C. (2012), "Analysis of steel-reinforced concrete-filled steel tubular (SRCFST) columns under cyclic loading", *Construction and Building Materials*, **28**(1), 88-95.

Doran B, Koksa H O, and Turgay T (2009), "Nonlinear finite element modeling of rectangular/square concrete columns confined with FRP", *Journal of Materials and Design*, **30**(8), 3066-3075.

Ehab, E. and Ben, Y. (2006), "Design and behavior of concrete-filled cold formed stainless steel tube columns", *Eng Struct*, **28**(5), 716-28.

Eurocode 4 (2004), *Design of composite steel and concrete structures, part 1.1, general rules and rules for building*, British Standards Institution, London, UK.

Han, L.H., Wang, W.D. and Zhao X.L. (2008), "Behavior of steel beam to concrete-filled SHS column frames, Finite element model and verifications", *Engineering Structures*, **30**(6), 1647-1658.

Hu, H.T., Huang, C.S. and Chen, Z.L. (2005), "Finite element analysis of CFT columns subjected to an axial compressive force and bending moment in combination", *Journal of Constructional Steel Research*, **61**(12), 1692-1712.

Lee, J. and Fenves, G. L. (1998). "Plastic-damage model for cyclic loading of concrete structures", *Journal of Engineering Mechanics*, **124**(8), 892-900.

Lu, F.W., Li, S.P. and Sun, G.J. (2007), "Nonlinear finite element analysis of square concrete-filled steel tube columns under compressive", *Engineering Mechanics*, **24**(3), 110-114. (in Chines)

Lubliner, J., Oliver, J., Oller, S. and Oñate, E. (1989), "A plastic-damage model for concrete", *International Journal of Solids and Structures*, **25**(3), 229-326.

Mander, J., Priestley, M. and Park, R. (1988), "Theoretical stress-strain model for confined concrete", *J. Struct. Eng*, **114**(8), 1804-1826.

Qi, H., Guo, L., Liu, J., Gan, D. and Zhang, S. (2011), "Axial load behavior and strength of tubed steel reinforced-concrete (SRC) stub columns", *Thin-Walled Structures*, **49**(9), 1141-1150.

Rougiera, V.C. and Luccionia, B.M. (2007), "Numerical assessment of FRP retrofitting systems for reinforced concrete elements", *Engineering Structures*, **29**(8), 1664-1675.

Shakir-Khalil, H. and Mouli, M. (1990), "Further tests on concrete-filled rectangular hollow-section columns", *The Structural Engineer*, **68**(20), 405-13.

Shanmugam, N.E. and Lakshmi, B. (2001), "State of the art report on steel-concrete composite columns", *Journal of Constructional Steel Research*, **57**(10), 1041-80.

Tao, Z., Uy, B., Liao, F.Y. and Han, L.H. (2011), "Nonlinear analysis of concrete-filled square stainless steel stub columns under axial compression", *Journal of Constructional Steel Research*, **67**(11), 1719-1732.

Tokgoz, S. and Dundar, C. (2010), "Experimental study on steel tubular columns in-filled with plain and steel fiber reinforced concrete", *Thin-Walled Structures*, **48**(6), 414-422.

Uy, B. (2001), "Strength of short concrete filled high strength steel box columns", *J Constr. Steel Res.*, **57**(1), 113-34.

Wang, Q., Zhao, D. and Guan, P. (2004), “Experimental study on the strength and ductility of steel tubular columns filled with steel-reinforced concrete”, *Engineering Structures*, **26**(7) ,907-915.

Yu, Q., Tao, Z. and Wu, Y.X. (2008), “Experimental behavior of high performance concrete-filled steel tubular columns”, *Thin-Walled Structures*, **46**(4), 362-370.

Zeghiche, J. (1988), “Concrete-filled composite columns”, M.Sc. Dissertation, University of Manchester, Manchester.

Zhang, X.P. (2001), *Nonlinear Analysis for RC Structure*, Science Press, Beijing, China. (in Chinese)

Zhao, D.Z., Wang, Q.X. and Guan, P. (2005), “Research on load-bearing capacity of steel tubular columns filled with steel-reinforced high-strength concrete subjected to compression and bending”, *Ind. Constr.*, **35**(9), 84-93. (in Chines)

Zheng, W. and Ji, J. (2008), “Dynamic performance of angle steel concrete columns under low cyclic loading-I, experimental study”, *Earthquake Engineering and Engineering Vibration*, **7**(1), 67-75.